Ion-beam focusing by self-organized axis-symmetric potentials in insulating capillaries

Eric Giglio, S. Guillous, A. Cassimi

Ion beam focusing by self-organized axis-symmetric potentials in insulating capillaries

E. Giglio, S. Guillous, and A. Cassimi
Centre de Recherche sur les Ions, les Matériaux et la Photonique (CIMAP), F-14000, Caen, France, EU

In a combined theoretical and experimental study, we give evidence that the self-organized electric potential in tapered glass capillaries has the strength to focus a low energy ion beam. Similar to Einzel lenses, the on-axis injected beam is focused by an axis-symmetric potential, generated by the charge accumulated in the insulating capillary . We argue that, for capillaries with large aspect ratio, the mechanism responsible for the focusing in our experiment is different from the one shown in earlier experiments. We found that the potential inside the capillary had to reach about 70% of the extraction potential of the ions source in order to be strong enough to focus the beam through the capillary. For higher intensities, the transmitted current density is shown to increase to a factor 10 with respect to the injected one. An original experimental setup is used to monitor the accumulated total charge in the capillary and link it to the transmitted fraction of the beam. This way, we can clearly identify the different stages of the transmission in real time, and in particular the Coulomb blocking, and explain why it occurred inevitable in this setup. The experimental data are corroborated by our simulations, which allow a valuable and comprehensive insight into the dynamics of the self-organized Coulomb potential. The latter controls the focusing effect, and explains many features such as why the transmitted fraction increases with the injected intensity.

PACS numbers: 34.80.Dp, 34.80.Pa

I. INTRODUCTION

Ion beam transmission through insulating capillaries and their surprising guiding power has been intensively studied since its discovery by Stolterfoht *et al.* for nano-capillaries and by Ikeda *et al.* for macroscopic glass capillaries [1–10, 12–17]. An interesting feature that has been highlighted in [6–10], is the ability of insulating tapered capillaries to compress the injected beam, resulting into a current density of the transmitted beam that is higher than the current density of the injected beam.

One distinguishes two mechanisms responsible for the enhanced transmitted current density. They differ by the symmetry of the accumulated charged distribution in the capillary wall. The first is due to a *non* axis symmetric charge deposition. For example, an injected ion beam, tilted with respect to the symmetry axis of the capillary, creates one or more local charge patches that guide the ions. The patches generate an electric field, which is stronger the closer to the charge patches. As a result, trajectories close to the charge patches are more deviated than trajectories farther away, resulting into a compression of the beam in one dimension. This compression mechanism, which is illustrated in Fig.1, takes place rather quickly after beam injection (see inset of Fig.1), as *transverse* fields become efficient to deflect the beam after only a relatively small amount of charge has been accumulated in those patches. Indeed, in our simulation (Fig.1), the beam compression takes place for a potential inside the capillary as low as 14 V, which is well below the extraction potential of the ion source of 3 kV. In the following, we refer to this mechanism as the transverse field compression.

The second mechanism is due to an axis-symmetric charge accumulation, generating an axis-symmetric potential in the capillary, which focuses the injected beam through the capillary outlet. The beam is compressed by the radial component of the electric field, similar to an electrostatic Einzel lens. We found in a preliminary numerical investigation, presented in [18], that the potential has to approach 70% of the extraction potential of the ion source in order to focus the injected beam through the outlet of an insulating conical shaped capillary. The radial focusing and the transverse compression differ thus not only by the symmetry of the charge accumulation in the capillary wall, but also on the hight of the self organized potential needed to became efficient. In the following, we refer to this mechanism as the radial focusing.

As noted before, for radial focusing to become efficient, two conditions must be fulfilled. The potential inside the capillary must (i) approach the extraction potential of the injected ions and (ii) have axial symmetry. Now, if one pays close attention to the setup and measured data in [6–9], which used tapered glass capillaries with large aspect ratio (length/diameter) around 70, one observes that at least one of the two requirements for radial focusing were not fulfilled in those experiments. In the case of [6, 8, 9], the observed compression was obtained for tilted capillaries with respect to the beam axis, which clearly favours local patch formation but hinders axis-symmetric charge accumulation. Also, they found that the transmission increased immediately after beam injection. This is the expected behaviour for transverse compression but not for radial focusing, as will be shown later in the manuscript. A minimum in the transmitted fraction was even found by [6, 8] for zero-tilt angle. In [7], a compression of a factor 10 of the injected beam was obtained after only 10 pC were accumulated in the tapered capillary, yielding an estimated potential inside the capillary of about 10 V. Clearly, the latter is insufficient for radial focusing of a 8keV Ar^8+ beam, but sufficient for trans-

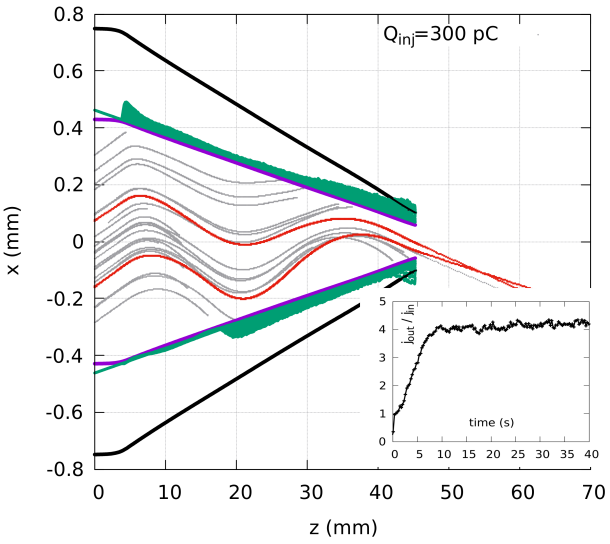

FIG. 1: Illustration of the transverse field compression of an injected ion beam by non axis symmetric deposited charge patches in a tapered capillary of large aspect ratio: Full violet curve stands for the inner surface of an insulating capillary, black curve for its outer metallized and grounded surface. The green areas (darkk gray) give the accumulated charge at opposite sides at the inner surface in arbitrary units. Gray curves represent simulated trajectories of an Ar^+ beam at 3 keV and tilted by 0.8 deg with respect to the capillary axis. The injected current is 30 pA. After only 300 pC have been stored at the inner capillary surface, the transmitted beam is compressed by a factor $j_{\rm out}/j_{\rm in} \simeq 4$ by the x-component of the electric field, as highlighted by the two red transmitted trajectories. Here, the highest value of the potential inside the capillary is 15 V, much too low for radial focusing. The inset shows the time-evolution of the transmitted current density $j_{\rm out}$ normalized with respect to the injected current density $j_{\rm in}$.

verse compression. The tilt angle was not mentioned. More specifically, in the case of [6], the outer surface of the borosilicate capillary was grounded, hindering the rise of the potential inside the capillary to the necessary 400 V (60% of the extraction potential) for an injected beam of 0.1 pA. The observed compression of a factor 2.5 found in [6] is thus preferably attributed to transverse compression, too. In [9], the capillary was exposed to stray electrons, as shows the extremely short charge decay rate of 4 minutes given in Fig. 3 of [9]. Based on the discussions in [11], we expect thus stray electron to hinder the rise of the potential inside the capillary to the necessary 60% of the extraction potential for radial focusing. In [7, 8], the screening of the capillary from stray electrons is never mentioned so that we can assume that a strong neutralization stray electron channel was also present in their experiment. For all these reasons, we exclude radial focusing as the mechanism to explain the compression found by the authors [6–9]. On the other hand, the transverse compression mechanism, illustrated in Fig 1 is clearly fitted to explain the observed beam compression found in [6–9]. A particular case represents the short capillary (14 mm) used by [10], with a 90keV, O^{6+}, 600pA ion beam. They found a transmitted current density which was 4.5 times larger than the injected one, and was maximal at zero tilt angle. For such short capillaries with an aspect ratio 3 to 4 times lower than the one we consider here, transverse compression is probably inefficient, so that the enhanced transmission was indeed due to radial focusing. However, the particular shape of the capillary used by [10] differs clearly from the capillary of large aspect ratio we consider in this study and will be analysed separately in a future work.

Following the above discussion, we estimate that focusing by axis symmetric self-organized potential, has not been demonstrated up to now in tapered insulating capillaries with large aspect ratio (> 50). The ability of insulating capillaries to focus an ion beam, in the sense of an Einzel lens, is referred to by the authors as the focusing power (by analogy with guiding power) of insulating tapered capillaries. Experimental and theoretical studies about the self-organized focusing power in insulating capillaries have been little documented. The reason probably is that the transmission through tapered glass capillaries is difficult to stabilize if there is no efficient leakage channel that keeps the capillary at low potential. Indeed, if the potential rises in the capillary, the ions are slowed down after entering the capillary. In the presence of a non-axis symmetric charge deposition, the ions are now easily deflected by possible transverse fields. This explains why the transmission becomes easily chaotic and unstable with increasing potential in long capillaries. Eventually, the beam is deflected into the capillary walls and the transmission blocks, even if the potential is still below the extraction potential of the source. Only by imposing an axis symmetric charge deposition can the transmission be stabilized in the absence of strong discharge channels. In this theoretical and experimental study, we give evidence that the charge deposited in tapered insulating capillaries by a singly-charged ion beam, can indeed generate an axis-symmetric electric field that is strong enough to focus the injected beam through the capillary. Details of the underlying mechanisms as well as general trends are explained with the help of our simulations.

II. EXPERIMENTAL SETUP

We designed a capillary holder that allows monitoring the time-evolution of the total electric charge stored in the capillary. The latter indicates if and when an equilibrium has been reached for which the leakage current balances the deposited current such that the charge stored in the capillary is stationary. It also indicates if and when the charge stored in the capillary approaches the critical charge for which the capillary focuses efficiently the beam through the outlet. Last but not least, it tells if a blocking of the transmission is due to Coulomb-blocking

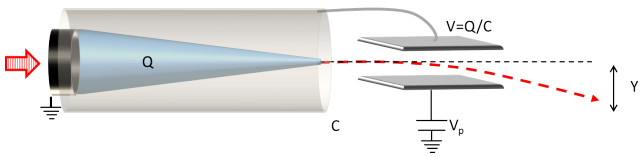

FIG. 2: A tapered glass capillary is surrounded by a cylindrical capacitor C, with the inner electrode electrically connected to the upper plate of a pair of deflection plates and the outer electrode grounded (not shown). Due to total influence, the potential $V = Q/C$ of the upper plate rises with the charge Q in the capillary. The transmitted beam is deflected by the electric field between the plates and the deflection Y monitored on a position sensitive detector. The potential V_p allows to deflect the beam using an external source. Usually V_p is put to zero during the measurements.

or due to a charge patch that deviates the beam into the capillary walls. In order to monitor the accumulated charge in the capillary, a cylindrical capacitor surrounds the capillary, with the outer cylinder grounded (Fig. 2). The inner cylinder is electrically connected to the upper plate facing a grounded plate. In this configuration, the capacity of the inner cylinder is $C = 13 \pm 0.2$ pF. Due to total influence, the potential V of the floating inner cylinder of the capacitor and upper plate rises with the charge stored in the capillary, $V = Q/C$. An electric field builds up between the two plates with increasing potential V, deflecting the transmitted beam that passes through the plates. For low angles, the deflection ΔY, measured on a position sensitive detector (PSD) located 270 mm downstream, is thus proportional to the charge stored in the capillary. The proportionality factor is deduced from calibration measurements and is equal to 88 ± 3 pC/mm for this setup. The whole acts as a perfect coulomb-meter. Particular attention has also been paid to screen the capillary, capacitor and the deflection plates from stray electrons. The latter would otherwise be attracted by the positive potential of the capillary and limit the rise of the potential in the capillary [11]. The capillary, capacitor and the deflection plates are therefore put into a larger grounded cylindrical box that screens them from outer stray electrons. The surrounding box has three inlets, one for the capillary, one for the Faraday cup and one with a grid pattern that together with the PSD allows measuring the emittance of the beam. It has also a 30x10 mm^2 large outlet to let pass the transmitted beam. Behind the outlet, we added a grid-less negatively biased electrode repeller, to avoid that low energetic stray electrons can enter the box. The holder can be heated in order to increase the conductivity of the capillary, for example, to speed up the discharge of capillaries. The holder is mounted on a high precision rotatable and translational plate, allowing for a alignment of the capillary axis with the beam axis by less than 0.1 degrees, by adjusting the elevation and azimuthal angles. Upstream, the beam is collimated by a plate with a 2 mm hole. The plate is connected to an ammeter and the intensity recorded, allowing in the later analysis to account for the fluctuation of the intensity of the source. Our capillary is homemade by pulling a locally heated borosilicate glass tube. Much attention was paid to get a axis symmetric straight capillary so as to ensure an axis symmetric charge deposition at zero tilt angle. The capillary is 74 mm long and the inner diameter of the entrance is 1.05 mm and that of the outlet is 144 µm. The shape of the inner surface of the capillary $R(z)$ is given by the violet curve in Fig. 5. The ratio between the outer and inner radius of the capillary was found constant and equal to 1.45. The first 11 mm of the outer surface are grounded. In front of the capillary is a grounded collimator with a hole of 0.6 mm diameter. The rms emittance of the injected Ar^+ beam of 2300 eV is about 0.1 mm.mrad and the divergence is about 0.15 degree (full opening angle). The pressure in the experimental chamber was 10^{-7} mbar. As the alignment of the capillary with the beam axis is crucial for axis-symmetric charge deposition, we used the following procedure for fine tuning the alignment: The capillary is heated to 70° C (343 K) in order to increase its charge relaxation rate. Close to alignment, some of the ions that are neutralized by hitting the inner surface are transmitted, forming a circle on the PSD, see Fig.3. In our case, the tapered capillary yields a circle that has a diameter of 6 mm. Some neutrals that are produced upstream pass also without hitting the capillary wall and produce a small spot on the PSD that falls within the circle but not necessarily on the origin (center) of the circle. We fine tune the alignment until the spot lies on the origin of an uniformly intense circle. This gives us an alignment within an error bar of ±0.05 deg. We retest the alignment once the capillary has cooled down to room temperature. The measurements were performed at room temperatures at the CIMAP laboratory in Caen, France.

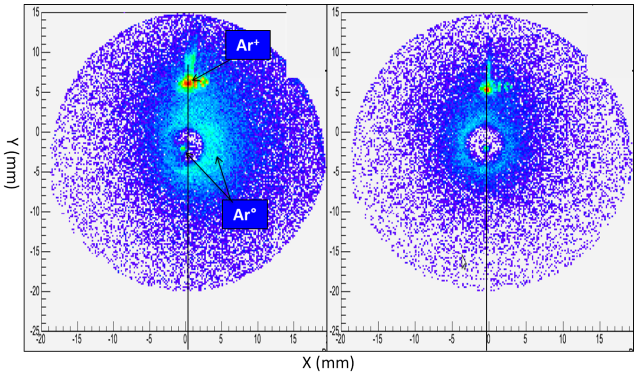

FIG. 3: Left: Ring of Ar neutrals on the PSD before fine-tuning the alignment. Spot of neutrals is off-centered and the ring is not uniformly intense. The transmitted ions Ar^+ were deflected upwards. Right: Uniformly intense ring of neutral with centered spot after rotating the capillary by the 0.12 degree (azimuthal angle). The vertical black line shows the alignment of the ion beam spot with the neutral spot before and after fine-tuning.

III. NUMERICAL MODEL

We developed in house a numerical code, called *InCa4D*, that simulates trajectories of the beam ions through an axis symmetric capillary. The dimensions of the capillary in the code are the same than the one used in the experiment, with the first 11 mm of the outer surface grounded. The model assumes that a projectile of charge q that hit the inner capillary surface injects q elementary charges (hole) at the interface. It assumes further that the charge accumulates only at the interfaces and not in the bulk, so that the charges stored in the capillary are described by two surface charge distributions, σ_1 and σ_2 at the inner $\vec{s}_1$ and outer $\vec{s}_2$ capillary interfaces. As a result, the electric field in the bulk is divergenceless, $\vec{\nabla}\cdot\vec{E}$. In borosilicate, the charge carriers are mobile alkali ions. The latter are field driven from the inner to the outer interface by the normal component E_n of the electric field, as well as along the inner and outer interface. The charge dynamics of both surface charge distributions is given by the surface continuity equation,

$$\frac{\partial\sigma_1}{\partial t} = -\kappa_b E_n(\vec{s}_1) - \kappa_s\vec{\nabla}_s\cdot\vec{E}(\vec{s}_1) + \gamma^h \quad (1)$$

$$\frac{\partial\sigma_2}{\partial t} = \kappa_b E_n(\vec{s}_2) - \kappa_s\vec{\nabla}_s\cdot\vec{E}(\vec{s}_2) + \gamma^e \quad . \quad (2)$$

The sources terms γ^h stands for the injected holes at the inner surface and γ^e for the injected electrons at the outer surface. In our simulation, γ^e was taken zero as the capillary holder in our setup screens the capillary from stray electrons. The operator $\vec{\nabla}_s\cdot$ is the surface divergence [23]. The current density along the interface is proportional to the surface conductivity κ_s, while the current density through the bulk is proportional to the bulk conductivity κ_b of the capillary. The model has thus two free parameter, κ_b and κ_s which need to be adjusted. The outer accumulated surface charges are eventually depleted by flowing along the outer interface to the grounded part of the capillary, where they are neutralized. Additionally to the two glass-vacuum interfaces of the capillary, the code accounts for a third interface S_3, namely the interface of a metal cylinder surrounding the capillary. The potential of the latter is floating and stands for the inner cylindrical electrode of the capacitor found in the the experimental setup. This way, the boundary conditions of the electric potential in the model are the same than those in the experimental setup. The dielectric constant $\epsilon_r = 4.6$ of the borosilicate glass is also taken into account by computing explicitly the polarisation charges $\sigma_1^{\rm pol}$ and $\sigma_2^{\rm pol}$ at the inner and outer glass-vacuum interfaces. The induced surface charges σ_3 at the metal cylinder interface are calculated by satisfying the appropriate boundary conditions at S_3. Finally, the divergenceless electric field is deduced from the potential V, which is obtained by integrating the charge distribution $\tilde{\sigma}_1 = \sigma_1 + \sigma_1^{\rm pol}$, $\tilde{\sigma}_2 = \sigma_2 + \sigma_2^{\rm pol}$ and $\tilde{\sigma}_3 = \sigma_3$ over the respective three interfaces S_1, S_2 and S_3,

$$V(\vec{s}_i) = \sum_{j=1}^{3}\int_{S_j}\frac{\tilde{\sigma}_j\,{\rm d}a_j}{4\pi\varepsilon_0\,|\vec{s}_j-\vec{s}_i|} \quad (3)$$

$$\vec{E}(\vec{s}_i) = -\frac{\partial V}{\partial\vec{s}_i} \quad , \quad (4)$$

with ${\rm d}a_j$ being the surface element of the $j^{\rm th}$ interface. Because the charges are computed only at the three interfaces, our approach is CPU cost efficient while keeping a realistic description of the charge transport in capillaries. In addition, as the boundary conditions at the 3 interfaces match the experimental ones, the numerical code is expected to reproduce with high accuracy the experimental electric field in the capillary and make reliable quantitative predictions. A typical simulation (10^6 trajectories), as presented in this paper, takes about 36 hours on a modern CPU core.

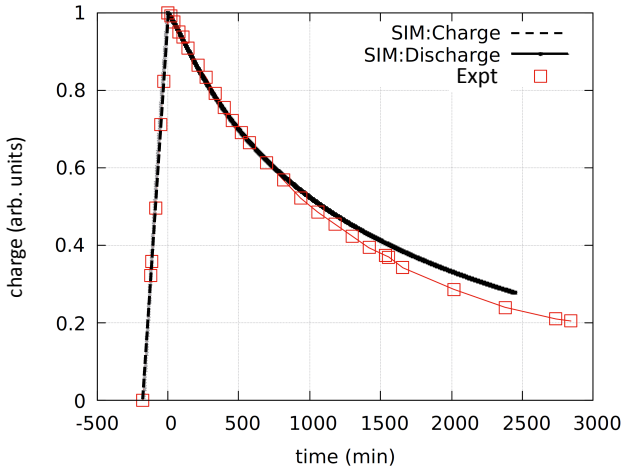

FIG. 4: Comparison between the experimental (red boxes) and simulated (gray and black lines) charge-discharge curve of our capillary. Best agreement was obtained for a bulk conductivity of $\kappa_b = 1.8\times10^{-15}$ S/cm and surface conductivity $\kappa_s = 2.6\times10^{-17}$ S.

In a first step, we want to determine the surface and bulk conductivity of the capillary used in the holder. As our setup allows measuring the accumulated charge as a function of time, we performed charge-discharge measurements of our capillary at room temperature (28°C), see Fig.4. First, the capillary is charged until $\sim$ 2 nC have been accumulated. Then, the holder is shifted by 1 cm, so as to present a 10µm hole to the beam. The transmitted beam passes through the deflector plates and monitors, via the ΔY deflection, the charge stored in the capillary. In this particular setup, an experimental depletion rate of about $\tau^{-1} = 0.012$ mHz was found. We want to emphasize that the observed depletion rate depends on the capacity C of the cylindrical electrode that surrounds the capillary. We remind that in our our setup

$C = 13 \pm 0.2$ pF. The measurements were then simulated with our code. To ensure a one to one comparison between the simulations and the experiment, cylindrical electrode of same capacity surrounded the capillary in the simulations. A surface conductivity $\kappa_s = 2.6 \times 10^{-17}$ S and bulk conductivity $\kappa_b = 1.8 \times 10^{-15}$ S/cm, in agreement with the measurements in [14], were found to reproduce at best the experimental discharge curve. Simulations, presented in this work, were done using those adjusted conductivities.

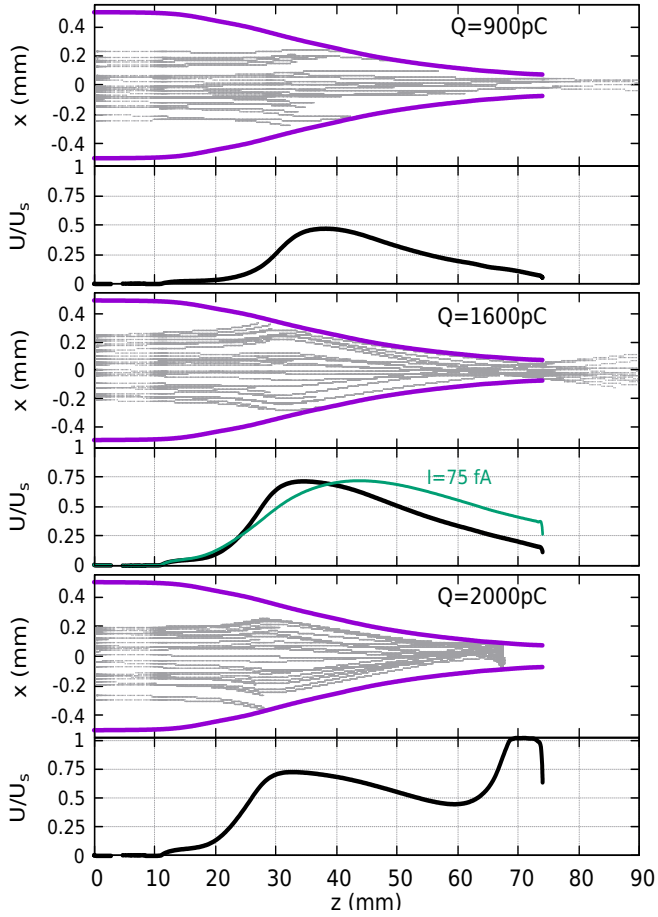

FIG. 5: Each snapshot, identified by the amount of charge Q stored in the capillary wall, is divided into two panels. The upper panel shows the ion trajectories (gray lines) through the capillary. The radius $R(z)$ of the inner surface of the capillary is represented by a violet (dark grey) full line. The lower panel show the Coulomb potential $U(z)$ at the inner capillary surface. The potential $U(z)$ is normalized with respect to the extraction potential $U_s = 2300V$ of the ions source. The green curve (labelled $I = 75$ fA), obtained for an injected current of 75 fA, has been added for comparison. For all the other curves, the injected current was 210 fA.

IV. SIMULATIONS

The trajectories of the injected ions coupled to the charge dynamics at the interfaces are calculated as a function of time. The focusing power of a tapered glass capillaries is shown in Fig. 5. The injected Ar^+ ions have an intensity of $I_{\rm in} = 210$ fA and the beam is aligned with the capillary's symmetry axis (zero tilt angle). The initial phase-space distribution of the injected ions are chosen such as to match the experimental emittance of the beam. The snapshots give the trajectories of the injected ions for different amounts of charge stored in the capillary. Below each snapshot we show the corresponding potential at the inner surface. For the initially discharged capillary, only 5.3% of the injected ions are transmitted, corresponding to the geometrical transmission, corrected by the divergence of the beam. Most ions hit the inner surface and charge the capillary inner wall. With increasing charge stored in the capillary, $Q = 900$ pC, the trajectories are slightly focused by the electric potential in the capillary and the transmission doubles to 10%. The potential U in the capillary attains, at his highest value, already 1100 V, which corresponds roughly to half of the extraction potential $U_s = 2300$ V of the ion source. Once about $Q = 1600$ pC are stored in the capillary, the electric potential inside the capillary is strong enough to focus the beam at the outlet. The transmission fraction $I_{\rm out}/I_{\rm in}$ reaches a maximum of 60% (which corresponds to a focusing factor of 11), resulting in a transmitted maximum current $I_{\rm out}^{\rm max}$ of 124 fA. The latter is obtained for a potential U inside the capillary of about $0.75 \times U_s = 1725$ V at its apex. Without surprise, the potential has its maximum where most of the charges are deposited, in the region where the inner diameter of the capillary equals the diameter of the inlet aperture. From the relation $\vec{\nabla} \cdot \vec{E} = 0$, it results that the focusing radial field E_r is strong there, where the negative curvature (second derivative) of the potential along the z-axis is large,

$$E_r(R(z), z) = \frac{1}{R(z)} \int_0^{R(z)} r \frac{\partial^2 V}{\partial z^2} dr \quad . \qquad (5)$$

In the middle panel of Fig. 5, the maximum of the focusing radial field is thus located around $z = 30$ mm. The accumulated charges in the capillary relax at a rate τ_r^{-1} dominated by the bulk conductivity

$$\tau_r{}^{-1} = \frac{\kappa_b}{\varepsilon_0 \varepsilon_r} \quad . \qquad (6)$$

The relaxation rate $\tau_r^{-1} \simeq 4.4$ mHz is not to be confused with the depletion rate $\tau^{-1} = 0.012$ mHz determined in the former discharge measurement and which characterizes the leakage current and which depends on the experimental setup. Now, the ratio, injected current over relaxation rate, $I_{\rm in}/\tau_r^{-1}$, directly controls the steepness of the self-organized potential along the z-axis and thus its curvatures. The higher the value of $I_{\rm in}\tau_r$, the steeper

the variation of the potential along the z-axis and consequently the stronger its focusing power. This trend is illustrated by the flatter but not necessarily lower green curve, which is obtained for an injected current of only 75 fA and yields a transmission factor of barely 24%. The trend will be discussed more in details in the text section. Note that the capillary behaves similar to an Einzel lens, where the focal point is moved from infinity towards the outlet of the lens with increasing potential of the central electrode and with decreasing distance between the central and outer grounded electrodes [22].

The leakage current depends on the conductivity of the glass and increases with the accumulated charge in the capillary. At maximum transmission (Q = 1600 pC), the leakage current is estimated to be about $Q/\tau \simeq$ 42 fA. Even then, the deposited charge per time unit, $I_{\rm in} - I_{\rm out}$ = 85 fA, still dominates the leakage current and the capillary continues to charge. As a result, the focusing distance continues to shorten and the focusing point enters the capillary tip. Part of the trajectories emerging from the focus point inside the capillary are now intercepted by the capillary walls and the potential rises quickly near the outlet. If the potential inside the capillary exceeds the potential of the ion source, the transmission blocks. In the lower panel of Fig.5 (Q = 2000 pC), the potential at the last 5 mm exceeds the source potential U_s of 2300 V and the ions u-turn at this point. This Coulomb blocking is inevitable, except of course if the deposited current is balanced by the leakage current before the potential in the capillary exceeds the source potential. Only then can a stable transmission be expected. Nevertheless, this theoretical study clearly shows that insulating tapered capillaries can be used to focus a low energetic ion beam.

V. EXPERIMENTAL RESULTS

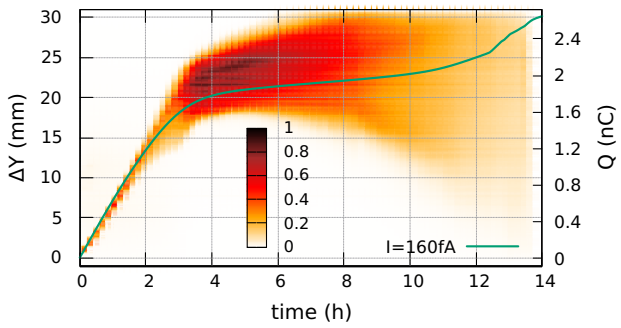

FIG. 6: Color online: Y-projection of the transmitted beam on the PSD as a function of time. Colours indicate the normalized counts per second per area of the beam spot. The full green (gray) curve gives the simulated time-evolution of the charge Q stored in the capillary for an input current of 160 fA. The right scale is the accumulated charge, using the relation Q[nC] = 0.088 × ΔY[mm], defined in the text.

Figure 6, shows the y-projection of the transmitted beam spot on the PSD as a function of time for an injected intensity of 160 ± 7 fA. The deflection of the transmitted beam translates into the charge stored in the capillary using the relation $Q(t)$[pC]= 88 × $\Delta Y(t)$[mm]. Initially, the spot on the detector has a size of less than 1 mm and is deflected vertically with increasing accumulated charge. After 2 hours of charging, the beam spot starts to spread, indicating that the focusing point approaches the outlet of the capillary. 2 hours later, the electric field in the capillary is strong enough to focus the beam at the outlet, resulting into a high transmitted fraction of 50%, which is indicated by the darker colors. The spot has now a size of 7 mm corresponding to a full opening angle of 1.5 degree, close to the full opening angle of the capillary of around tan(1.05/45) = 1.4 degree. At this point, the total deflection of 21 mm indicates that the capillary accumulated a total charge of about 1.8 nC. A high transmission of more than 80 fA is kept for about 4 hours before the transmission slowly fades away. During the high transmission, the beam spot continues to spread, while its center rises only slowly. The latter indicates that a quasi balance between the deposited and leakage current is attained. We add in Fig. 6 the simulated time-evolution of the accumulated charge $Q(t)$ in the capillary (full green curve) for a same input current of 160 fA. From the slope of the curve between 4h and 8h, we deduce that the capillary continues to accumulate charge at a rate of 15 fA. This low accumulation rate explains the long stable transmission for over 4 hours. Still, after 13 hours, a charge of 2100 pC has been accumulated and the transmission stops, because of Coulomb blocking. Monitoring the accumulated charge in the capillary is crucial for analysing and clearly identifying the different stages of the transmission dynamics, especially from the perspective to stabilize the transmission.

In a second step, we studied the transmitted beam intensity $I_{\rm out}$ for six different injected beam intensities $I_{\rm in}$, ranging from 75 to 210 fA. The experimental results are given in the upper panel of Fig.7. Note the typical time-evolution of the transmitted fraction in the case of radial focusing, which differs strongly from the one in the case of transverse focusing (see inset of Fig.1). Only after at least 800 pC have been stored in the capillary walls, does the transmission increases rapidly from the initial geometrical fraction. We found that the focusing factor increases from 4 to 10, or alternatively, the transmission fraction $I_{\rm out}/I_{\rm in}$ increased from 20% to 50% with the increasing intensity. For injected intensities less than 120 fA, the beam was transmitted for more than 24 hours and no Coulomb blocking was observed for the time of the experiment. In these cases, we know from the ΔY deviation of the spot on the PSD that the charge in the capillary never exceeded 2100 pC, which corresponds to the critical value for which the potential in the capillary is expected to exceed the source potential. For currents above 120 fA, the charge accumulated in the capillary during the time of the experiment was sufficient to gener-

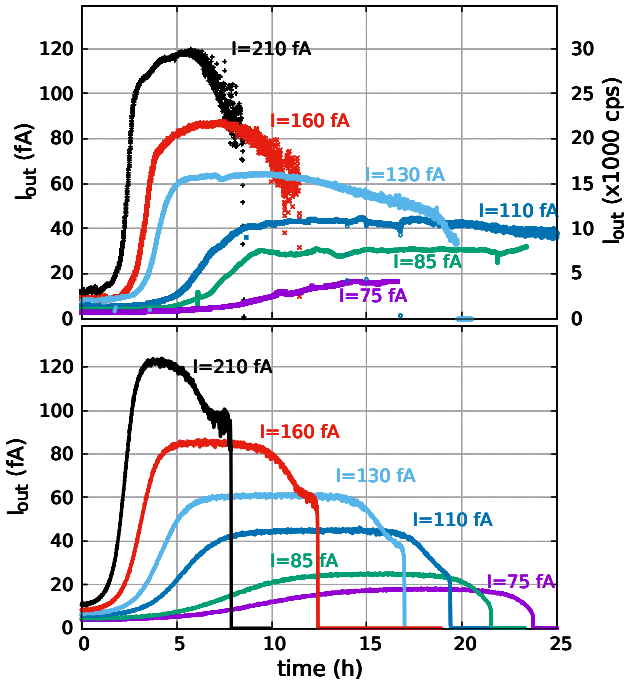

FIG. 7: The transmitted intensity I_{out} through the glass capillary as a function of time, for 6 different injected intensities ranging from 75 to 210 fA. Top panel: Experimental data. The transmitted intensity passing through a transmission grid of 10% is measured on the PSD and expressed in counts per second (cps), as indicated by the right vertical scale. Assuming an efficiency of the detector of 40%, the left vertical scale gives the transmitted intensity in fA. Bottom panel: Theoretical transmitted current, simulated with our numerical code *InCa4D* using the parameters defined in section II.

ate a potential that exceeds the source potential and the transmissions faded slowly away. In these cases, the leakage current was too small to compensate for the deposited charge per time unit. Increasing the conductivity of the capillary (for example by heating) will certainly allow for higher input currents without experiencing Coulomb blocking.

We simulated for the same intensity range the transmission and compared it to the experimental data (lower panel of Fig.7). Simulations corroborate the experimental findings that the transmission fraction increased with the intensity. The quantitative agreement is remarkable, giving great confidence in the predictions that can be calculated by our model. This was made possible by developing the capillary holder, while keeping in mind that the boundary conditions imposed on the electric field in the capillary and its holder must be matched by our the numerical code. The simulations also corroborate that, with our particular experimental setup, the injected current always dominates the leakage current, so that the high transmission cannot be maintained and the Coulomb blocking not avoided. The numerical code offers thus a valuable tool to test the effect of different beam or capillary parameters on the stability of the transmission. For example, a lower beam emittance, was found to allow stable high transmissions for longer times. Such studies are under work.

The simulations also confirm the trend that, at the apex of the transmission, the rise of the self-organized potential along the z-axis is steeper for higher intensities. As a result, the potential exhibits a larger negative curvature, which yields a stronger focusing radial electric field (see eq. 5). Now, for axis symmetric charge distributions at the capillary interfaces, the radial component of the electric field E_r is strong mainly outside of the capillary interfaces and should be very weak inside, even if non-zero. It is thus interesting to show E_r inside the capillary at the moment the transmission is maximal. In Fig.8, the axis symmetric radial field $E_r(r = R(z), z)$, taken at the inner surface $R(z)$ of the capillary, is given for different injected current intensities. Negative values have a radial focusing effect while positive values have a defocusing effect. The focusing part of the field between 26 and 40 mm always dominates the preceding defocusing part and increases with increasing current intensity. This explains why focusing power and thus transmission fractions increases with higher injected currents. While the intensity of the focusing part of the fields are indeed weak, (< 10 V/mm), they are sufficient to focus a 2300 keV Ar^+ beam through the capillary outlet.

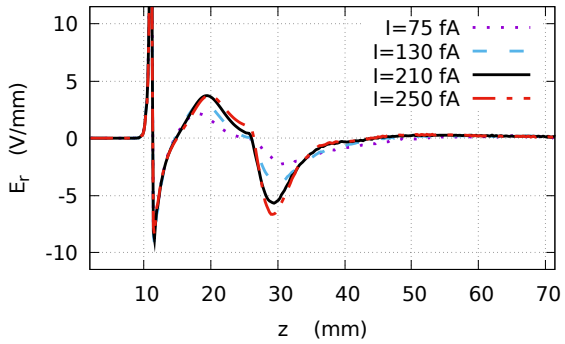

FIG. 8: color online: Radial electric field $E_r(r = R(z), z)$ at the inner surface inside the capillary, taken at the apex of the transmission, for different injected current intensities. Negative values have a radial focusing effect while positive values have a defocusing radial effect. Note that the fast fluctuation of the field around 11 mm is due to the negative charge accumulation at the grounded outer electrode, which covers the first 11 mm of the outer capillary surface. It has only a negligible effect on the ion trajectories and is irrelevant here.

VI. CONCLUSION

In this paper, we described experimentally and theoretically the charge dynamics in tapered insulating capil-

laries and demonstrated the focusing power of the resulting self-organized potential for zero tilt angle. With our original capillary holder, that allows monitoring the accumulated charge in the capillary, we succeed to describe the different stages of the transmission. We deduced the leakage current at the apex of the transmitted beam and showed that is too low, compared to the deposited current, to maintain a stable transmission. Nevertheless, for intensities below 120 fA, the transmission was stable for more than 24 hours. Simulations show that the injected beam is efficiently focused through the outlet if the self-organized potential of our capillary approaches 75% of the extraction potential of the ion source. For a given electrical conductivity of the capillary, the self organized potential is steeper with increasing injected intensity, resulting in a higher focusing radial electric field. We could thus explain the observed trend that the transmitted fraction increases with the injected beam intensity. We showed that our simulations are in excellent quantitative agreement with the experimental data, giving us much confidence in the underlying model. The reliable and comprehensive predictions of the simulations will be of immense help to improve and stabilize the transmission, boosting the interest of ion beam transport by tapered glass capillaries.

Acknowledgments

This work was funded by the French National Research Agency (ANR) in the P2N 2012 program (ANR-12-NANO-008) for the PELIICAEN project. We thank Claire Feierstein for designing and building the capillary puller, Sylvain Girard for its computer interface and Emmanuel Gardès for the emittance meter.

[1] N. Stolterfoht, J.-H. Bremer, V. Hoffmann, R. Hellhammer, D. Fink, A. Petrov, and B. Sulik, Phys. Rev. Lett. **88** (2002) 133201.
[2] K. Schiessl, W. Palfinger, K. Tőkési, H. Nowotny, C. Lemell, and J. Burgdörfer, Phys. Rev. A. **72** (2005) 062902.
[3] A.R. Milosavljević, Gy. Víkor, Z. D. Pesić, P. Kolarz, D. Sević, and B. P. Marinković, S. Mátéfi-Tempfli, M. Mátéfi-Tempfli, and L. Piraux, Phys. Rev. A **75** (2007) 030901(R).
[4] H.F. Krause, C. R. Vane, and F. W. Meyer, Phys. Rev. A **75** 042901 (2007)
[5] K. Schiessl, K. Tőkési, B. Solleder, C. Lemell, and J. Burgdörfer, Phys. Rev. Lett. **102** (2009) 163201.
[6] E. Gruber, N. Stolterfoht, P. Allinger, S. Wampl, Y. Wang, M. J. Simon, F. Aumayr, Nuclear Instruments and Methods in Physics Research B 340 (2014) 14
[7] T. Ikeda, Y. Kanai, T. M. Kojima, Y. Iwai, T. Kambara, and Y Yamazaki, M. Hoshino, T. Nebiki and T. Narusawa, Applied Phys. Lett. **89** (2006) 163502.
[8] M. Kreller, G. Zschornack, and U. Kentsch, Nucl. Instr. and Meth. Phys. Res. B **269** (2011) 1032
[9] A. Cassimi, T. Ikeda, L. Maunoury, C. L. Zhou, S. Guillous, A. Mery, H. Lebius, A. Benyagoub, C. Grygiel, H. Khemliche, P. Roncin, H. Merabet, and J. A. Tanis, Phys. Rev. A **86** (2012) 062902.
[10] Jing Chen, Nucl. Inst. and Meth. Phys. Res. B **281** (2012) 2629
[11] E. Giglio, S. Guillous, A. Cassimi, H. Q. Zhang, G. U. L. Nagy, and K. Tőkési, Phys. Rev. A 95, 030702(R) (2017)
[12] P. Skog, H. Q. Zhang, and R. Schuch, Phys. Rev. Lett. **101** (2008) 223202.
[13] R.J. Bereczky, G. Kowarik, F. Aumayr, and K. Tőkési, Nucl. Instr. and Meth. Phys. **B267** (2009) 317.
[14] E. Gruber, G. Kowarik, F. Ladinig, J. P. Waclawek, D. Schrempf, F. Aumayr, R. J. Bereczky, K. Tőkési, P. Gunacker, T. Schweigler, C. Lemell and J. Burgdörfer, Phys. Rev. A **86** (2012) 062901.
[15] C. Lemell, J. Burgdörfer, F. Aumayr, Progress in Surface Science **88** (2013) 237.
[16] N. Stolterfoht, E. Gruber, P. Allinger , S. Wampl, Y. Wang, M. J. Simon, and F. Aumayr, Phys. Rev. A **91** 032705 (2015).
[17] N. Stolterfoht and Y. Yamazaki Physics Reports **629**, (2016) 1
[18] E. Giglio, R.D. Dubois , A. Cassimi and K. Tőkési , Nucl. Instr. and Meth. Phys. Res. B **354** (2015) 82
[19] S. Guillous *et al.* Rev Sci Instrum. (2016) 87(11):113901.
[20] T. Ikeda *et al.* Surface and Coatings Technology **206** (2011) 859.
[21] Iwai *et al.*, Appl. Phys. Lett. 92, (2008) 023509
[22] Heddle, D W O (2000), Electrostatic Lens Systems, Bristol and Philadelphia: IOP Publishing Ldt 2000
[23] W. McAllister, IEEE Transactions on Electrical Insulation Vol. 26 No. 3, (1991)